



C. Tanikawa  
K. Takada

## Objective classification of nose–lip–chin profiles and their relation to dentoskeletal traits

### Authors' affiliations:

C. Tanikawa, Department of Orthodontics, Graduate School of Dentistry, Center for Advanced Medical Engineering and Informatics, Osaka University, Osaka, Japan

K. Takada, Discipline of Orthodontics and Paediatric Dentistry, Faculty of Dentistry, National University of Singapore, Singapore, Singapore

### Correspondence to:

Dr. Kenji Takada  
Faculty of Dentistry  
National University of Singapore  
11 Lower Kent Ridge Road  
Singapore 119083  
Singapore  
E-mail: denkt@nus.edu.sg

Tanikawa C., Takada K. Objective classification of nose–lip–chin profiles and their relation to dentoskeletal traits

*Orthod Craniofac Res* 2014; **17**: 226–238. © 2014 John Wiley & Sons A/S. Published by John Wiley & Sons Ltd

### Structured Abstract

**Objectives** – To objectively classify the nose–lip–chin profiles of adult women and identify any associations between the nose–lip–chin profile patterns and dentoskeletal patterns.

**Setting and Sample Population** – Lateral facial photographs and lateral cephalograms were obtained for 229 Japanese women who were being assessed for orthodontic treatment.

**Methods** – A feature vector that was effective in distinguishing differences in nose–lip–chin profiles was extracted for each photograph. To categorize the records into an optimum number of subclasses according to nose–lip–chin profile configurations, a vector quantization method was applied to the feature vectors of all samples. Dentoskeletal patterns that corresponded to the nose–lip–chin profile subclasses were compared.

**Results** – Eight profile patterns were identified, and the differences among patterns were notably maximized by the nasolabial angle, configuration and vertical length of the subnasal region, vertical thickness of the lip vermilion borders, sagittal position of the upper- and lower-lip vermilion borders and their relation to each other, labiomental angle, depth of the labiomental sulcus, degree of prominence of the chin, and degree of protrusion of the mandible. The dentoskeletal patterns showed significant differences between the classified profile patterns ( $p < 0.01$ ).

**Conclusions** – A method to objectively classify the nose–lip–chin profiles of adult women was established, and the nose–lip–chin profile patterns were found to be associated with the dentoskeletal patterns.

**Key words:** classification; facial profile; vector quantization

## Introduction

Traditionally, human facial profiles have been classified into certain types of pattern (e.g., convex, straight, and concave) (1)

### Date:

Accepted 30 April 2014

DOI: 10.1111/ocr.12047

© 2014 John Wiley & Sons A/S.

Published by John Wiley & Sons Ltd

on the basis of intuition or tacit knowledge, which was considered as implicitly correct. Ricketts (2) qualitatively classified facial profiles into 10 patterns based on the relationship of the lips with the esthetic plane. The ‘classification’ or ‘taxonomy’ of facial profiles is convenient for clinical use because of their simplicity and convenience in rapidly interpreting facial profiles, but also it gives us access to structured information on patients with similar profiles. Such a classification would enable optimization of soft-tissue-based diagnosis and treatment planning in orthodontics. Despite clinical demands, thus far, few attempts have been made to examine objectively the optimal number of facial profile patterns.

Previous studies have recommended the use of specific soft-tissue parameters as facial profile descriptors for cephalometric (3–7) and photographic (8–10) analyses. Although conventional linear and angular measurements are useful for understanding local features of the facial form, they have limitations such as being fragmental and thus are often unsuitable for a holistic understanding of the overall features (*e.g.*, a concave profile with a moderately prominent chin or a ‘dished-in’ profile). Entire facial profiles have been evaluated using the Fourier transformation (11–13). This mathematical technique is clinically useful for approximating human facial profiles, but to date, no system has been established that employs facial descriptors to categorize the profiles into more than two groups. Recently, a vector quantization (VQ) method (14) has been employed to give a holistic understanding of the overall features of human nose (15) and lip vermilions (16). In this method, combinations of variables that represent facial profiles were dealt with as multidimensional vectors and human nose and lip vermilion configurations were categorized based on their vector similarities.

Analyzing the shape of the nose and the lip vermilion separately at high resolution is vital for detecting the subtle and local morphological traits that can be indispensable when designing optimum treatment plans for improving facial esthetics. Thus, it is desirable to compartmentalize the

facial profile into several anatomically defined segments for the purposes of detailed analysis. However, the practitioner must also have a holistic understanding of the facial profile, *that is*, the section from the base of the nose to the chin as an integrated unit.

Therefore, the present study aimed (1) to classify objectively the various soft-tissue profiles of adult women into several distinct patterns that reflect a holistic representation of human facial configurations using the VQ method and (2) to examine whether the classified soft-tissue profiles are associated with any of the morphological characteristics of the dentoskeletal patterns.

## Material and methods

### Material

Conventional two-dimensional lateral facial photographs (right-side views) and standard lateral cephalograms were obtained, before treatment, from 229 Japanese females (mean age, 26 years and 2 months; age range, 18 years and 2 months to 59 years and 1 month) who had been registered to the orthodontic patient list at the university dental hospital. Patients were enrolled consecutively in order of registration. The criteria for selection were permanent dentition; aged between 18 and 60 years; no congenital anomalies; and no history of surgery, trauma or injury to the face. Digital conventional photographs and cephalograms were taken with the teeth in habitual maximum intercuspation position and the lips in repose. For photography, a camera equipped with a 2.3-megapixel effective CCD sensor (FinePix 2900Z; Fuji Film, Kanagawa, Japan) and a 70-mm telescopic lens was employed.

### Data acquisition

For each photograph, the positions of 11 facial landmarks [*sellion* (*se*), *exocathion* (*ex*), *porion* (*po*), *pronasale* (*prn*), *subnasale* (*sn*), *labial superior* (*ls*), *stomion* (*sto*), *cheilion* (*ch*), *labial inferior* (*li*), *supramental* (*sm*), and *cervical neck* (*cn*)] were located visually (17). The positions of

two facial landmarks [*gnathion* (*gn*) and *subgnathion* (*gn*<sup>\*</sup>)] were mathematically defined because these landmarks were hard to locate visually in patients exhibiting chin retrusion (Table 1). A set of multiple points (mean, 553 points; range, 322–1125 points) that constituted the contour of the facial profile from the forehead to the inferior part of the chin was identified automatically using customized software (15). After these contour data were imported into a new coordinate system for standardization (see Fig. 1), the set of x- and y-coordinates describing the facial profile located between the y-coordinates of *prn* and *gn* was segmented and

**Table 1. Definitions of soft-tissue landmarks (17)**

Soft-tissue landmark	Definition
<i>Sellion</i> ( <i>se</i> )	Deepest point of the naso-frontal angle
<i>Exocathion</i> ( <i>ex</i> )	Point at the commissure of the eye fissure
<i>Porion</i> ( <i>po</i> )	Most superior point on the ear rod
<i>Pronasale</i> ( <i>prn</i> )	Most prominent point on the tip of the nose
<i>Subnasale</i> ( <i>sn</i> )	Midpoint of the angle at the columella base where the lower border of the nasal septum and surface of the upper lip converge
<i>Labial superior</i> ( <i>ls</i> )	Point that indicates the mucocutaneous limit of the upper lip
<i>Stomion</i> ( <i>sto</i> )	Point on the horizontal labial fissure
<i>Cheilion</i> ( <i>ch</i> )	Point located at the labial commissure
<i>Labial inferior</i> ( <i>li</i> )	Point that indicates the mucocutaneous limit of the lower lip
<i>Supramental</i> ( <i>sm</i> )	Deepest point of the inferior sublabial concavity
<i>Cervical neck</i> ( <i>cn</i> )	Deepest point along the chin–neck contour (R point)
<i>Gnathion</i> ( <i>gn</i> ) <sup>*</sup>	Most antero-inferior point of the chin profile with respect to a line connecting <i>sto</i> and <i>cn</i> (mathematically defined point)
<i>Subgnathion</i> ( <i>gn</i> ) <sup>*</sup>	Most anterior point of the chin profile with respect to a line connecting <i>sm</i> and <i>gn</i> (mathematically defined point)
<i>g</i> point	Geometric centroid point of <i>po</i> , <i>sn</i> , and <i>ex</i> (mathematically defined point)

\*New definitions used for the present study.

used as a nose–lip–chin profile. In addition, a lip profile between *ls* and *li* was segmented and used as a lip vermilion configuration (16), with lines that connected *ch* and *sto*, *ch* and *ls*, and *ch* and *li*.

To examine the craniofacial morphological characteristics of the patients, 12 cephalometric variables were measured for each cephalogram. The dentoskeletal traits of the patients are summarized in Appendix S1 (18, 19) (Table S1).

#### Data analysis

Figure 2 presents an overview of the classification procedure employed in this study.

Step 1: Generation of a combination of variables representing the nose–lip–chin profile (i.e. a feature vector) for each patient

Thirteen variables that described various morphological traits of the soft-tissue profile were selected. (For details regarding selection of variables, see Appendix S2; for definitions of these variables, see Table 2 and Fig. 3). In addition to the aforementioned variables, a subset of variables that represented the lip vermilion configuration was employed to describe the nose–lip–chin profile. (For detailed calculations, see Appendix S3.)

These 13 variables and 1 variable subset were regarded as feature elements constituting a multidimensional feature vector that holistically described the configuration of the nose–lip–chin profile.

Step 2: Classification of nose–lip–chin profiles based on pattern similarities of feature vectors from the entire data set

To classify the nose–lip–chin profiles, a VQ method (14) was applied to the feature vectors extracted from the entire data set. The VQ method allows facial profiles, each expressed by a multidimensional vector, to be categorized based on their vector similarities. Centroids of each category were used as mean codes (i.e. patterns) that were assumed to represent each category. The mean nose–lip–chin profile of each category was reconstructed by averaging the curves and lines describing the facial profiles of patients in that category.

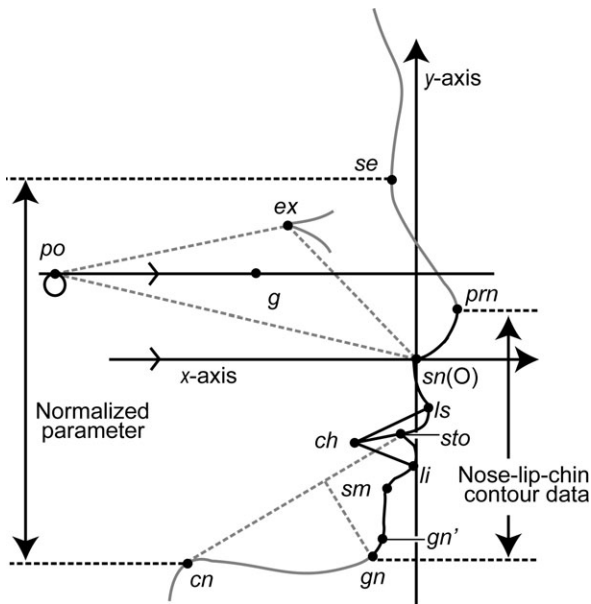


Fig. 1. Schematic diagram illustrating the segmentation of the nose–lip–chin contour data and the definition of the coordinate system. The *sn* was defined as the origin (O) of the system. The *x*-axis is defined as a line that passes through the origin and is parallel to a line connecting the *po* and point *g* (*po*–*g* line (15)). The *y*-axis was defined as a line perpendicular to the *x*-axis and passing through the origin. A set of *x*- and *y*-coordinates located between the *y*-coordinates of the *prn* and the *gn* points were extracted to form the nose–lip–chin contour data. The positions of the soft-tissue landmarks and the nose–lip–chin contour data were defined mathematically and normalized with respect to the difference in the *y*-coordinate values between the *se* and the *cn*.

**Statistics**

To compare classified nose–lip–chin profile patterns, a one-way ANOVA was performed for each variable (vector element) of the feature vectors

and for each cephalometric variable. In addition, a Tukey–Kramer *post hoc* test was used for multiple testing.  $p < 0.01$  was considered as statistically significant.

To determine the intra-observer reliability of the measurements, 15 images were randomly selected, and the measurement was repeated. Intraclass correlation coefficient (ICC) (20) was used to determine reliability between the repeated measurements.

**Results**

The ICC values for the intra-observer reliability ranged from 0.81 to 1.00 indicating excellent reliability. The optimal number of subclasses required to classify the subjects included in this study with regard to their nose–lip–chin profile was found to be eight. The proportion of subjects classified into each respective code, from Code 1 to Code 8, was 17.2%, 14.8%, 14.4%, 14.0%, 13.1%, 10.4%, 10.4%, and 5.7%, respectively. The mean nose–lip–chin patterns corresponding to each code are shown in Fig. 4. Statistically significant differences were found among the eight codes for all feature vector elements (Fig. 5).

The soft-tissue profile traits for each code are summarized in Table 3. As explained by feature vector element *v1*, codes 5 and 6 designate a re-truded mandible, whereas codes 7 and 8

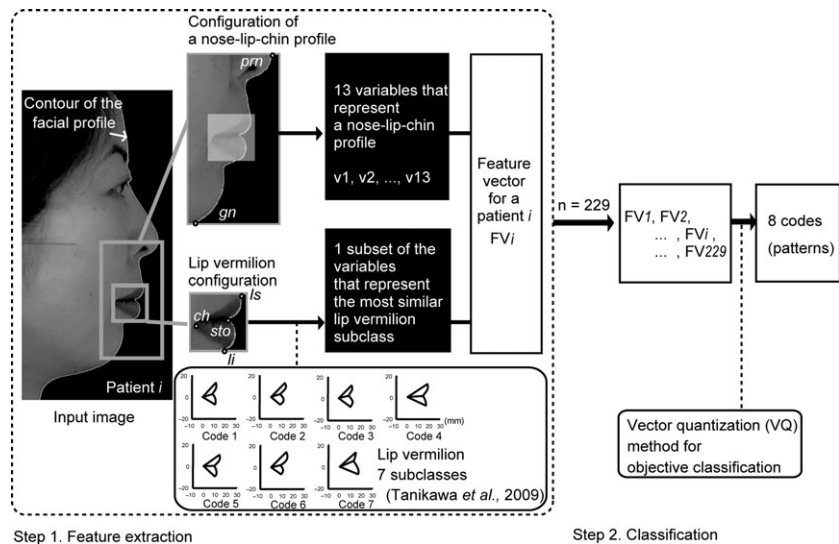


Fig. 2. Overview of the classification procedure employed in the present study.

**Table 2. Definitions and interpretations of 13 vector elements**

Vector element	Definition	Interpretation
v1	Angle formed by the <i>sn-gn</i> line and <i>x</i> -axis	Protrusive degree of the mandible. A large value indicates a more protruded mandible
v2	Angle formed by the <i>prn-sn</i> line and <i>sn-ls</i> line	Naso-labial angle
v3	Angle formed by the <i>li-sm</i> line and <i>sm-gn'</i> line	Labio-mental angle
v4	Angle formed by the <i>sm-gn'</i> line and <i>x</i> -axis	Degree of the chin prominence. A small value indicates a prominent chin
v5	(Difference between <i>y'</i> coordinate values of <i>sn</i> and <i>ls</i> ) / (Difference between <i>y'</i> coordinate values of <i>prn</i> and <i>gn</i> )	Vertical length of the subnasal region
v6	The <i>x'</i> coordinate value of <i>ls</i>	Sagittal position of the upper-lip vermillion. A positive value indicates a protruded upper lip relative to the line connecting <i>prn</i> and <i>gn</i>
v7	The <i>x'</i> coordinate value of <i>li</i>	Sagittal position of the lower-lip vermillion. A positive value indicates that the lower lip is protruded relative to the line connecting <i>prn</i> and <i>gn</i>
v8	(v6 + v7)	Sagittal position of the upper- and lower-lip vermilions. A positive value indicates bilabially protruded lip vermilions
v9	(v7 – v6)	Sagittal relationship of the upper and lower lips. A positive value indicates a more protruded lower lip relative to its upper counterpart
v10	Difference between <i>x'</i> coordinate values of <i>sn</i> and <i>sm</i>	Protrusive degree of the labio-mental sulcus
v11	Difference between <i>x'</i> coordinate values of <i>sm</i> and <i>li</i>	Depth of the labio-mental sulcus
v12	Angle formed by the approximated lines A and B, where the Line A was defined as an approximated line between <i>sn</i> and a midpoint of <i>sn</i> and <i>ls</i> ; the Line B was defined as an approximated line between a midpoint of <i>sn</i> and <i>ls</i> , and <i>ls</i>	Subnasal ( <i>sn-ls</i> line) form. A small value indicates a backward-curved subnasal form
v13	Difference between <i>y</i> coordinate values of <i>ls</i> and <i>li</i>	Vertical thickness of the lip vermilions

describe a protruded mandible ( $p < 0.01$ ). The naso-labial angle had significantly greater mean values in codes 1 and 4 than in Code 7 (v2;  $p < 0.01$ ). Codes 4 and 8 exhibited a significantly more prominent chin with a smaller labio-mental angle than codes 5 and 6 (v3, v4;  $p < 0.01$ ). The subnasal region of Code 2 had a significantly longer vertical height than Code 7 (v5;  $p < 0.01$ ).

Codes 7 and 8 had retruded upper-lip vermilions, whereas codes 5 and 6 showed protruded upper-lip vermilions (v6;  $p < 0.01$ ). Code 5 exhibited protruded lower-lip vermilions (from the line connecting the tip of the nose and the chin), whereas codes 4 and 8 showed retruded lower-lip vermilions (v7;  $p < 0.01$ ). Codes 5 and

6 represented bilabially protruded lip vermilions relative to the line connecting the nose and chin, whereas codes 4 and 8 exhibited retruded lip vermilions relative to the line connecting the nose and chin (v8;  $p < 0.01$ ). The lower lip in codes 5 and 7 was more protruded (relative to the line connecting the nose and chin) than the upper lip (v9;  $p < 0.01$ ). Codes 5 and 7 also exhibited a labio-mental sulcus in a forward position relative to the line connecting the nose and chin, whereas in Code 4, this sulcus was in a backward position (v10;  $p < 0.01$ ). Codes 7 and 8 were characterized by a small anteroposterior gap between the lower lip and the labio-mental sulcus, whereas in codes 2, 5, and 6, this gap was greater (v11;  $p < 0.01$ ).

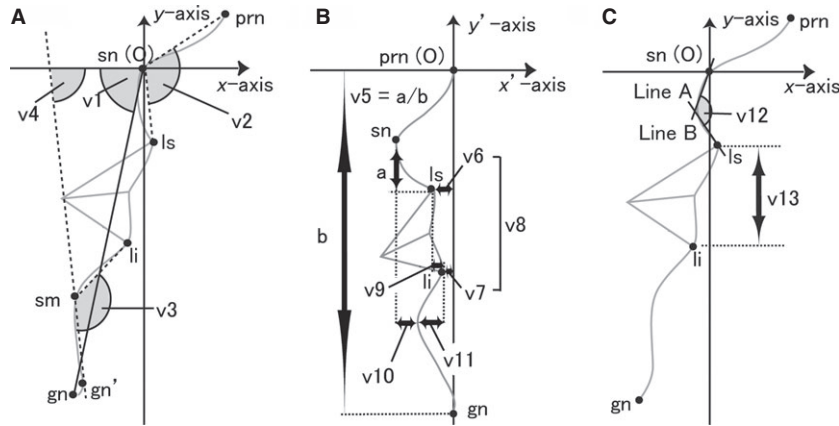


Fig. 3. Schematic diagram illustrating vector elements v1, v2, v3, and v4 (A); v5, v6, v7, v8, v9, v10, and v11 (B); v12 and v13 (C). The gray line denotes nose-lip-chin profile contour data. (A) See Fig. 1 for the coordinate system. (B) The *prn* is the origin. The *y'*-axis is the line connecting *prn* and *gn*; the *x'*-axis is the line perpendicular to the *y'*-axis passing through the origin. The data on the contour that were segmented between *prn* and *gn* were redefined mathematically. (C) See Fig. 1 for the coordinate system. Lines A and B are the 1st order polynomial approximations generated from the extracted contour data (for Line A, the data were extracted from *sn* to a midpoint of *sn* and *ls*; for Line B, the data were extracted from *ls* to a midpoint of *sn* and *ls*).

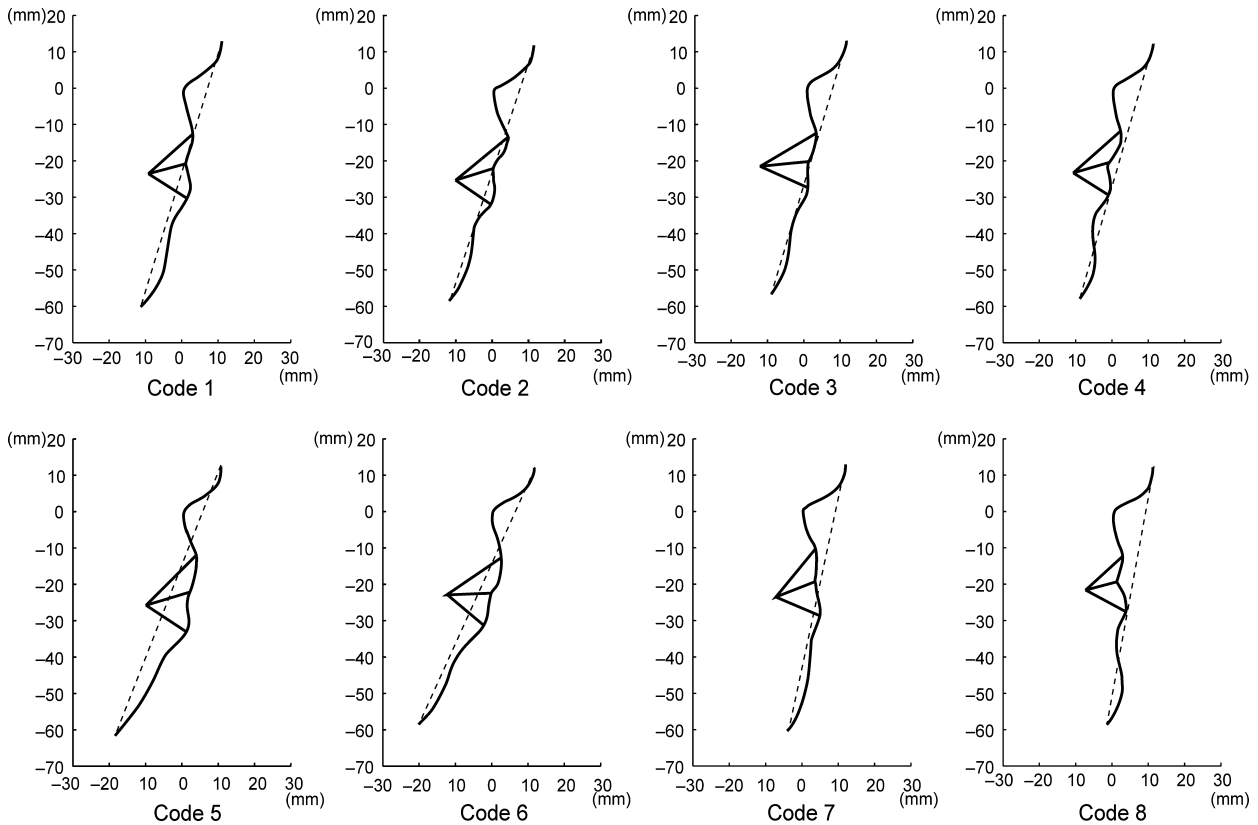


Fig. 4. Mean nose-lip-chin profiles that correspond to the eight codes (patterns). Origin, *sn*, *x*-axis, the line parallel to the line *po-g* passing through *sn*; *y*-axis, the line perpendicular to the *x*-axis through the origin. The dotted line connects *prn* and *gn*.

Code 6 exhibited a forward-curved subnasal (*sn-ls* line) form, giving a more round, ‘full’ mouth, whereas codes 2, 7, and 8 showed a backward-curved subnasal form (v12;  $p < 0.01$ ).

Codes 3, 4, and 8 designated a shorter vertical height of the lip vermilions (often called a ‘thin’ lip vermilion), whereas this height was longer in Code 5 (v13;  $p < 0.01$ ).

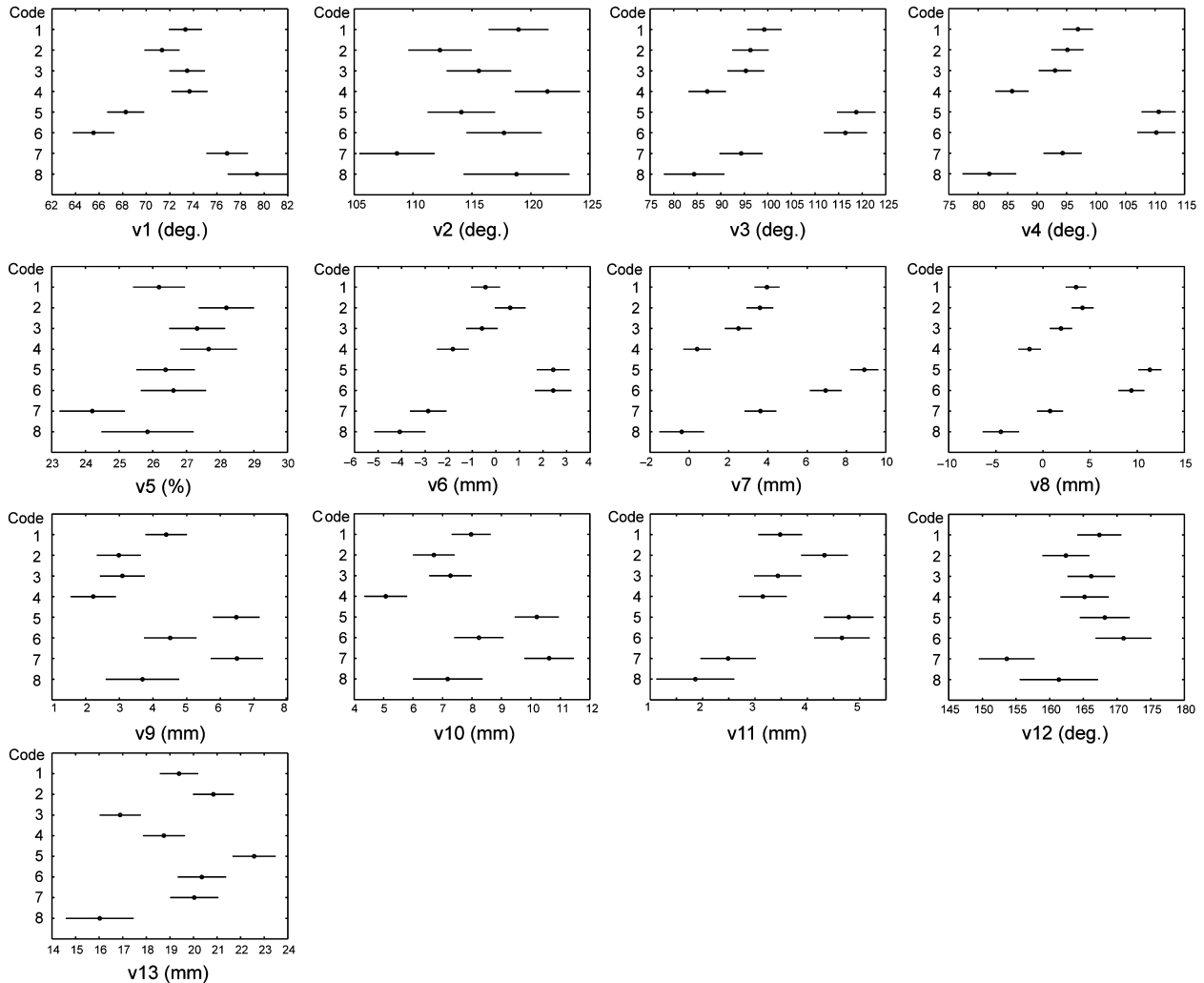


Fig. 5. Intercode comparisons of sample means calculated for each of the 13 feature vector elements. x-axis, vector element values expressed in real space; y-axis, code number. Error bars represent Tukey–Kramer comparison intervals: non-overlap between the bars of any two codes indicates that the hypothesis of no difference between the two was rejected at the  $p < 0.01$  level. Circle symbols represent estimated means.

Figure 6 gives statistical comparisons of the sample means between the groups corresponding to each classified soft-tissue code and for each of the dentoskeletal variables. Table 3 provides a summary of the dentoskeletal traits defining each respective code. These traits were determined statistically as being significantly eminent.

For the horizontal length of the anterior cranial base, Code 3 exhibited a significantly greater mean value than codes 1 and 4 (SN;  $p < 0.01$ ). Regarding the maxilla, no significant differences were found between any of the codes for the SNA angle or the maxillary length (SNA, A-Ptm/PP;  $p > 0.01$ ). Regarding the mandible, the mean

mandibular effective lengths were greater in codes 7 and 8 than in Code 6 (Ar-Me;  $p < 0.01$ ). Codes 5 and 6 exhibited significantly greater mean mandibular plane angles than codes 1, 2, 3, and 4 (SNMP;  $p < 0.01$ ), and Code 5 had a significantly greater mean anterior lower face height than Code 4 (Me/PP;  $p < 0.01$ ). As for the angle ANB, codes 7 and 8 had significantly smaller mean values than codes 5 and 6 ( $p < 0.01$ ).

With regard to upper incisor inclination, Code 7 exhibited a significantly greater mean U1-SN value than codes 4, 6, and 8 ( $p < 0.01$ ). For the lower incisors, codes 7 and 8 had significantly greater mean L1-FH values than codes 5 and 6 ( $p < 0.01$ ). Codes 2 and 6 showed significantly

**Table 3. Summary of the morphological features of the eight nose–lip–chin profile patterns and their corresponding dento-skeletal traits**

Code no.	Soft-tissue profile trait	Corresponding dentoskeletal trait
Code 1	<ul style="list-style-type: none"> <li>• Obtuse naso-labial angle</li> <li>• Lower-lip vermillion more protruded than its opponent</li> </ul>	<ul style="list-style-type: none"> <li>• Skeletal Class I</li> <li>• Long mandibular effective length</li> <li>• Long lower anterior face height</li> <li>• Reduced overjet and overbite</li> </ul>
Code 2	<ul style="list-style-type: none"> <li>• Large vertical height from <i>sn</i> to <i>ls</i></li> <li>• Heavily concaved subnasal (<i>sn-ls</i> line) form</li> <li>• Upper-lip vermillion more protruded than its opponent</li> <li>• Large horizontal gap between the lower lip and the labio-mental sulcus</li> </ul>	<ul style="list-style-type: none"> <li>• Skeletal Class I</li> <li>• Increased overjet; Incisor Class II</li> </ul>
Code 3	<ul style="list-style-type: none"> <li>• Short lip vermillion height (often called a 'thin' lip vermillion)</li> <li>• Anterior–posteriorly large lip vermilions</li> <li>• Lip fissure that goes upward posteriorly</li> </ul>	<ul style="list-style-type: none"> <li>• Skeletal Class I</li> <li>• Slightly long anterior cranial base length</li> <li>• Long mandibular effective length</li> </ul>
Code 4	<ul style="list-style-type: none"> <li>• Obtuse naso-labial angle</li> <li>• Short lip vermillion height (often called a 'thin' lip vermillion)</li> <li>• Retruded upper- and lower-lip vermilions from the line connecting the nose and the chin</li> <li>• Distinct labio-mental sulcus</li> <li>• Prominent chin with a smaller labio-mental angle</li> </ul>	<ul style="list-style-type: none"> <li>• Skeletal Class I</li> <li>• Upper incisors show a tendency toward palatal inclination</li> </ul>
Code 5	<ul style="list-style-type: none"> <li>• Protruded upper- and lower-lip vermilions (lower-lip vermillion more protruded than its opponent relative to the line connecting the nose and chin)</li> <li>• Vertically longer lip vermilions ('thick' lip vermilions)</li> <li>• Lip fissure that goes downward posteriorly</li> <li>• Large labio-mental angle</li> <li>• Retruded chin</li> </ul>	<ul style="list-style-type: none"> <li>• Skeletal Class II tendency</li> <li>• High angle</li> <li>• Long face</li> <li>• Labially inclined lower incisors</li> <li>• Reduced overbite</li> </ul>
Code 6	<ul style="list-style-type: none"> <li>• Forward-curved subnasal (<i>sn-ls</i> line) form (often referred to as a 'round full' mouth)</li> <li>• Protruded upper- and lower-lip vermilions from the line connecting the nose and the chin</li> <li>• Upper-lip vermillion more protruded than its opponent</li> <li>• Lip fissure that goes upward posteriorly</li> <li>• Large labio-mental angle</li> <li>• Retruded chin</li> </ul>	<ul style="list-style-type: none"> <li>• Skeletal Class II accompanied by a small mandibular effective length and a retruded mandible relative to the anterior cranial base</li> <li>• High angle tendency</li> <li>• Upper incisors show a tendency toward palatal inclination</li> <li>• Labially inclined lower incisors</li> <li>• Increased overjet</li> </ul>

**Table 3. (continued)**

Code no.	Soft-tissue profile trait	Corresponding dentoskeletal trait
Code 7	<ul style="list-style-type: none"> <li>• Acute naso-labial angle</li> <li>• Shorter vertical height from <i>sn</i> to <i>ls</i></li> <li>• Heavily concaved subnasal (<i>sn-ls</i> line) form</li> <li>• Retruded upper-lip vermilion and protruded lower-lip vermilions from the line connecting the nose and the chin</li> <li>• Lip fissure that goes downward posteriorly</li> <li>• Small horizontal gap between the lower lip and the labio-mental sulcus</li> <li>• Forward positioned labio-mental sulcus</li> <li>• Protruded chin</li> </ul>	<ul style="list-style-type: none"> <li>• Skeletal Class III accompanied by a long mandibular effective length and a protruded mandible relative to the anterior cranial base</li> <li>• Long face</li> <li>• Labially inclined upper incisors</li> <li>• Lingually inclined lower incisors</li> <li>• Reduced overjet</li> <li>• Reduced overbite</li> </ul>
Code 8	<ul style="list-style-type: none"> <li>• Heavily concaved subnasal (<i>sn-ls</i> line) form</li> <li>• Retruded upper- and lower-lip vermilions from the line connecting the nose and the chin</li> <li>• Lower-lip vermilion is more protruded than its opponent</li> <li>• Short lip vermilion height (often called a 'thin' lip vermilion)</li> <li>• Prominence of the chin with smaller labio-mental angle</li> </ul>	<ul style="list-style-type: none"> <li>• Skeletal Class III accompanied by a long mandibular effective length and a protruded mandible relative to the anterior cranial base</li> <li>• Lingually inclined lower incisors</li> <li>• Long face tendency</li> <li>• Reduced overjet</li> </ul>

increased mean overjets relative to codes 7 and 8 ( $p < 0.01$ ). The mean overbite was significantly reduced in Code 7 relative to codes 2, 3, 4, and 6 ( $p < 0.01$ ).

Figure 7 exemplifies cephalometric tracings of subjects in the current study who represent the morphological characteristics typical of the eight codes.

## Discussion

### Study settings

The sample in the present study was taken only from adults above 18 years of age because previous reports (3, 21) had shown that children and adolescents between 7 and 17 years of age have intense soft-tissue growth. In addition, we employed only female subjects to reduce any possible gender-related influences on facial morphology (22).

### Relationship between nose–lip–chin profiles and corresponding dentoskeletal forms

Because the soft-tissue facial profiles are significantly influenced by orthodontic and orthognathic surgical treatments (5, 23, 24), a structured or systematic knowledge of the relationship between the nose–lip–chin profile and its relationship to the underlying dentoskeletal form is crucial for orthodontic practitioners when making treatment plans. Interestingly, soft-tissue thickness is known to differ between patients with short faces and those with long faces (21, 25) and between patients who exhibit Class II and Class III malocclusions (22). This indirectly implies that there are facial soft-tissue morphological traits that are specific to dentoskeletal patterns. The soft-versus-hard-tissue relationship has been evaluated previously using Fourier (13) and principal component (26) analyses. These studies measured the accuracy of soft-tissue profile

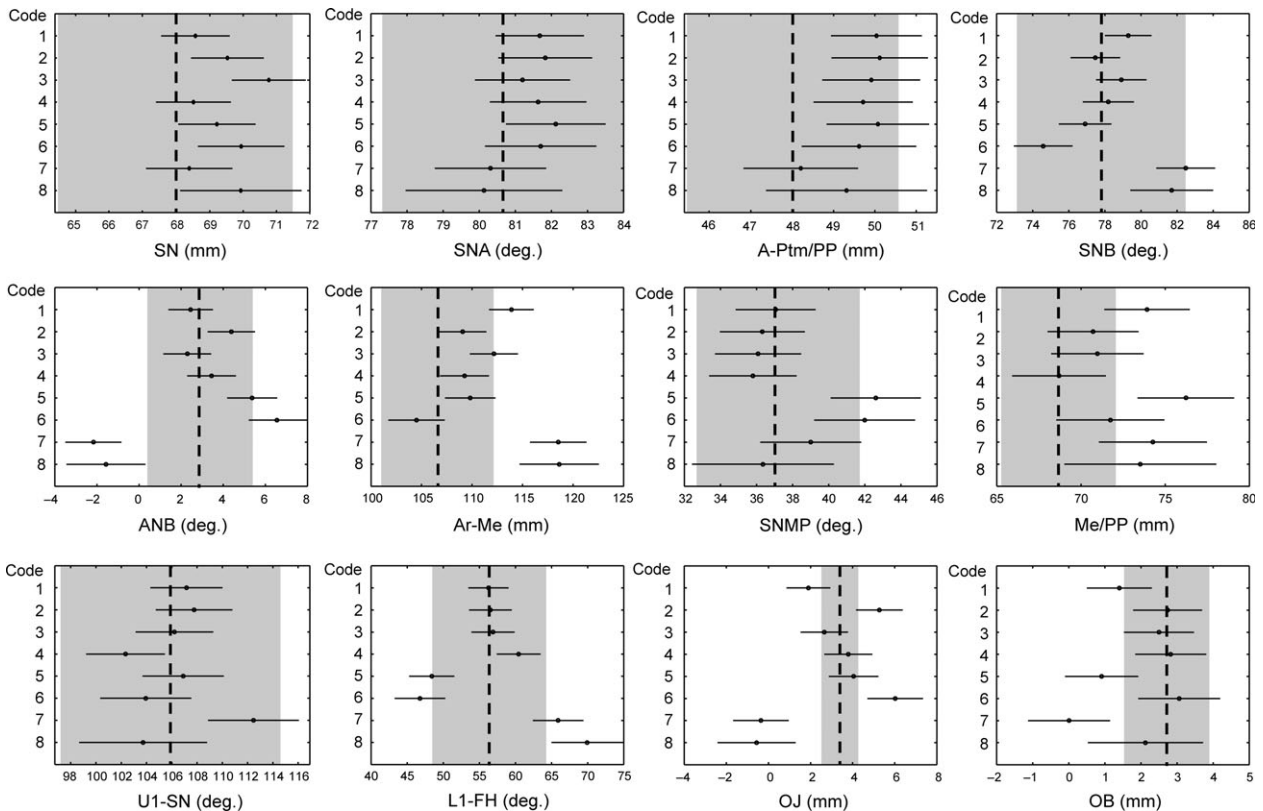


Fig. 6. Intercode comparisons of the sample means calculated for each of the 12 dentoskeletal variables. The  $x$ -axis denotes measured values, and the  $y$ -axis indicates the code number. Dotted lines represent the overall mean values for each variable (18). Shaded areas represent a range of plus/minus one standard deviation around the mean (18). Error bars represent Tukey–Kramer comparison intervals: Non-overlap between the bars of any two codes indicates that the hypothesis of no difference between the two was rejected at the  $p < 0.01$  level. Circle symbols represent estimated means.

contours reconstructed from hard tissue structures, and the latter (26) concluded that only 50% of the variability in soft-tissue shape was related to that of the underlying hard tissues. Furthermore, no significant associations between the skeletal classes and soft-tissue arrangements were found in a study (27) that examined Class I and II skeletal groups using a standardization method based on vertical facial height.

In the present study, we classified the samples into several groups by applying the VQ technique based on the morphological similarity of the soft-tissue facial profiles. The variances determined for each subgroup were smaller than that calculated for the entire sample (*i.e.*, the sum of the subgroups). Thus, it was possible to define the associations between hard and facial soft-tissue structures more accurately by referring specifically to the parameters of each group rather than the entire sample.

Whereas there was no significant association between the soft-tissue profile and the size and position of the maxilla, cephalometric variables relating to the mandible (*i.e.*, its horizontal/vertical position, posture and size) were found to be associated with the soft-tissue configuration. In particular, the vertical dimension was a key factor in discriminating facial features, as described below.

#### Class I profiles (Codes 1, 3, and 4)

Because codes 1, 3, and 4 exhibited a moderately protruded chin (See v1.), we assumed that they corresponded to a conventionally defined straight-type profile (28). Code 4 exhibited a greater naso-labial angle, a smaller labio-mental angle associated with a retruded labio-mental sulcus, a more prominent chin, and thin, retruded upper- and lower-lip vermilions. Overall, these

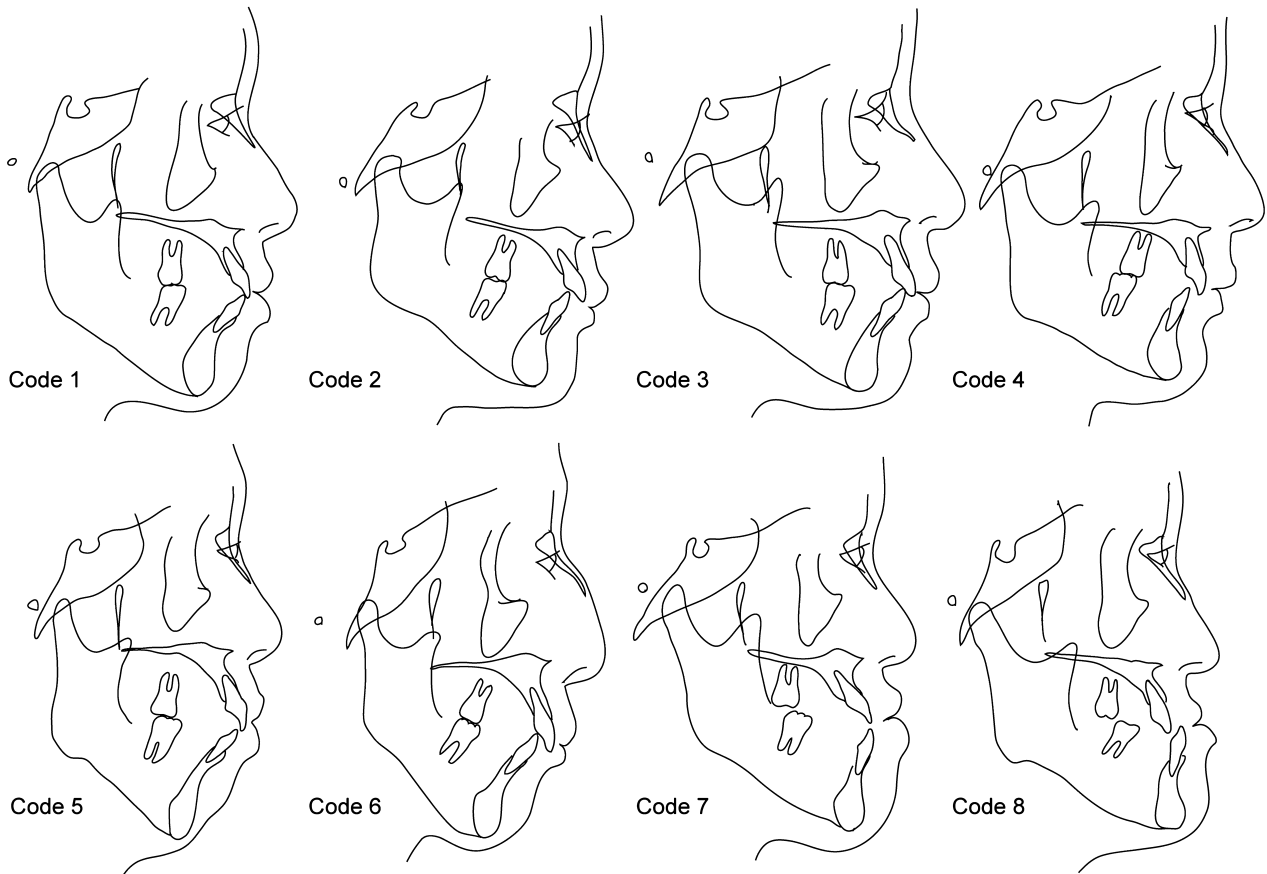


Fig. 7. Cephalometric tracings of patients exhibiting morphological traits typical of the eight codes.

characteristics are considered to represent a ‘dished-in’-type profile (29) and could be a manifestation of the corresponding skeletal characteristics of this profile, which include palatally and lingually inclined upper and lower incisors. These findings are consistent with previous findings (30, 31) that documented a significant decrease in the upper- and lower-lip vermilion heights caused by over-retraction of the incisors.

**Class II profiles (Codes 2, 5, and 6)**

Codes 5 and 6 had similar characteristics, that is, protruded upper- and lower-lip vermilions and less prominent chin. These codes were associated with skeletal Class II tendencies with high mandibular plane angles. Chin retrusion occurs as the mandible rotates clockwise. This forces the upper and lower lips into protruded positions relative to the chin. It should also be noted that both codes 5 and 6 exhibited verti-

cally long (‘thick’) vermilions. It has been assumed that vertical shortness of the cutaneous lips leads to increased vertical exposure of the vermilion lips (32). If we accept this assumption, it can be inferred that the inherent vertical cutaneous lip shortness associated with incongruity of the lip structure due to a clockwise-rotated mandible creates vertically longer vermilion lips.

In contrast, Code 2 exhibited morphological traits that were significantly different from the other Class II profiles (*i.e.*, prominent chin, retruded upper- and lower-lip vermilions, and more protrusion of upper lip than lower lip). The differences between Code 2 and the other Class II profiles can be explained with reference to the underlying skeletal morphological traits of the normal mandibular plane angle. The inclination of the mandible seems to be a critical factor determining the soft-tissue morphological differences between Code 2 and codes 5 and 6.

### Class III profiles (Codes 7 and 8)

The profiles of both codes 7 and 8 were characterized by a protruded mandible and retruded upper-lip vermilion. These traits describe the ‘concave’-type conventional facial profile subclass (28). When compared with Code 8, Code 7 exhibited a smaller naso-labial angle, a more protruded lower-lip vermilion (relative to the line connecting the tip of the nose and the chin), vertically longer (*i.e.*, ‘thicker’) lip vermilions, and a less prominent chin. The smaller naso-labial angle in Code 7 could be associated with labially inclined upper incisors. In addition, it can be speculated that the tendency toward a high mandibular plane angle and a relatively reduced overbite seen in Code 7 ( $p < 0.05$ ) could manifest as a poorly defined chin prominence and thicker lip vermilions.

### Clinical applications

In a previous study (33), a mathematical model that can predict the optimum treatment plans based on the pre-treatment conditions of orthodontic patients was developed. Another study (34) reported a mathematical model that can predict the locations of the anatomical landmarks on X-ray images. What is common in these two prediction models is that a large amount of data were accumulated as feature vectors, that is, mathe-

matical descriptions that explain clinical pictures, and the data most similar to a new input were employed for prediction. Similarly, it is expected that a database of the differences between pre- and post-treatment feature vectors that describe the configuration of the facial profile for patients having each subdivision determined in the present study will allow a computer-assisted artificial intelligent system to precisely predict post-treatment facial profiles before treatment.

It should be noted that the current objective classification method we have developed can be applied to various ethnic groups. This will enable the objective determination of the similarities or differences in the facial profiles of any ethnic group.

### Clinical relevance

In the present study, we newly established a method that enables to classify human facial profiles into several representative patterns objectively and quantitatively. The objective classification of facial profiles of each individual patient on the basis of our newly developed method should allow practitioners to develop more precise orthodontic treatment plans, taking into account possible post-treatment changes for each facial profile pattern.

### References

1. Proffit WR. *Contemporary Orthodontics*, 3rd edn. St Louis: Mosby; 2000.
2. Ricketts RM. Esthetics, environment, and the law of lip relation. *Am J Orthod* 1968;54:272–89.
3. Subtelny JD. A longitudinal study of soft tissue facial structures and their profile characteristics defined in relation to underlying skeletal structures. *Am J Orthod* 1959;45:481–507.
4. Merrifield LL. The profile line as an aid in critically evaluating facial esthetics. *Am J Orthod* 1966;52:804–22.
5. Burstone CJ. Lip posture and its significance in treatment planning. *Am J Orthod* 1967;53:262–84.
6. Holdaway RA. A soft-tissue cephalometric analysis and its use in orthodontic treatment planning. Part I. *Am J Orthod* 1983;84:1–28.
7. Arnett GW, Jelic JS, Kim J, Cummings DR, Beress A, Worley CM Jr et al. Soft tissue cephalometric analysis: diagnosis and treatment planning of dentofacial deformity. *Am J Orthod Dentofacial Orthop* 1999;116:239–53.
8. Stoner MM. A photometric analysis of the facial profile. A method of assessing facial change induced by orthodontic treatment. *Am J Orthod* 1955;45:481–507.
9. Peck H, Peck S. A concept of facial esthetics. *Angle Orthod* 1970;40:284–318.
10. Fernández-Riveiro P, Suárez-Quintanilla D, Smyth-Chamosa E, Suárez-Cunqueiro M. Linear photogrammetric analysis of the soft tissue facial profile. *Am J Orthod Dentofacial Orthop* 2002;122:59–66.
11. Halazonetis DJ, Shapiro E, Gheewalla RK, Clark RE. Quantitative description of the shape of the mandible. *Am J Orthod Dentofacial Orthop* 1991;99:49–56.
12. Tangchaitrong K, Messer LB, Thomas CD, Townsend GC. Fourier analysis of facial profiles of young twins. *Am J Phys Anthropol* 2000;113:369–79.
13. Rose AD, Woods MG, Clement JG, Thomas CD. Lateral facial soft-tissue prediction model: analysis using

- Fourier shape descriptors and traditional cephalometric methods. *Am J Phys Anthropol* 2003;121:172–80.
14. Chang PC, Gray RM. Gradient algorithms for designing predictive vector quantizers. *IEEE Trans Acoust Speech Signal Process* 1986;34:679–90.
  15. Tanikawa C, Kakiuchi Y, Yagi M, Miyata K, Takada K. Knowledge-dependent pattern classification of human nasal profiles. *Angle Orthod* 2007;77:821–30.
  16. Tanikawa C, Nakamura K, Yagi M, Takada K. Lip vermilion patterns and corresponding dentoskeletal forms in female adults. *Angle Orthod* 2009;79:849–58.
  17. Farkas L. *Anthropometry of the Head and Face*, 2nd edn. New York: Raven Press; 1994.
  18. Wada K. A study on the individual growth of maxillofacial skeleton by means of lateral cephalometric roentgenograms. *J Osaka Univ Dent Sch* 1977;22:239–69.
  19. Takada K, Lowe AA, Freund VK. Canonical correlations between masticatory muscle orientation and dentoskeletal morphology in children. *Am J Orthod* 1984;86:331–41.
  20. Shrout PE, Fleiss JL. Intraclass correlations: Uses in assessing rater reliability. *Psychol Bull* 1979;86:420–8.
  21. Blanchette ME, Nanda RS, Currier GF, Ghosh J, Nanda SK. A longitudinal cephalometric study of the soft tissue profile of short- and long-face syndromes from 7 to 17 years. *Am J Orthod Dentofacial Orthop* 1996;109:116–31.
  22. Utsuno H, Kageyama T, Uchida K, Yoshino M, Oohigashi S, Miyazawa H et al. Pilot study of facial soft tissue thickness differences among three skeletal classes in Japanese females. *Forensic Sci Int* 2010;195:165.
  23. Legan HL, Burstone CJ. Soft tissue cephalometric analysis for orthognathic surgery. *J Oral Surg* 1980;38:744–51.
  24. Erdinc AE, Nanda RS, Dandajena TC. Profile changes of patients treated with and without premolar extractions. *Am J Orthod Dentofacial Orthop* 2007;132:324–31.
  25. Mauchamp O, Sassouni V. Growth and prediction of the skeletal and soft-tissue profiles. *Am J Orthod* 1973;64:83–9.
  26. Halazonetis DJ. Morphometric correlation between facial soft-tissue profile shape and skeletal pattern in children and adolescents. *Am J Orthod Dentofacial Orthop* 2007;132:450–7.
  27. Ferrario VF, Sforza C. Size and shape of soft-tissue facial profile: effects of age, gender, and skeletal class. *Cleft Palate Craniofac J* 1997;34:498–504.
  28. Godt A, Muller A, Kalwitzki M, Goz G. Angles of facial convexity in different skeletal Classes. *Eur J Orthod* 2007;29:648–53.
  29. Drobocky OB, Smith RJ. Changes in facial profile during orthodontic treatment with extraction of four-first premolars. *Am J Orthod Dentofacial Orthop* 1989;95:220–30.
  30. Oliver BM. The influence of lip thickness and strain on upper lip response to incisor retraction. *Am J Orthod* 1982;82:141–9.
  31. Perkins RA, Staley RN. Change in lip vermilion height during orthodontic treatment. *Am J Orthod Dentofacial Orthop* 1993;103:147–54.
  32. Jacobs JD. Vertical lip changes from maxillary incisor retraction. *Am J Orthod* 1978;74:396–404.
  33. Takada K, Yagi M, Horiguchi E. Computational formulation of orthodontic tooth-extraction decisions. Part I: to extract or not to extract. *Angle Orthod* 2009;79:885–91.
  34. Tanikawa C, Yagi M, Takada K. Automated cephalometry: system performance reliability using landmark-dependent criteria. *Angle Orthod* 2009;79:1037–46.

## Supporting Information

Additional Supporting Information may be found in the online version of this article:

**Appendix S1.** Dentoskeletal morphological traits of the study sample.

**Appendix S2.** Selection of variables for measurement.

**Appendix S3.** Feature extraction from the lip vermilion configuration.

**Table S1.** Summary of dentoskeletal morphological traits of the present study samples.

Copyright of Orthodontics & Craniofacial Research is the property of Wiley-Blackwell and its content may not be copied or emailed to multiple sites or posted to a listserv without the copyright holder's express written permission. However, users may print, download, or email articles for individual use.